

Supplementary information:

Polarized emission of CdSe nanocrystals in magnetic field: the role of phonon-assisted recombination of the dark exciton

Gang Qiang, Aleksandr A. Golovatenko, Elena V. Shornikova, Dmitri R. Yakovlev, Anna V. Rodina, Evgeny A. Zhukov, Ina V. Kalitukha, Victor F. Sapega, Vadim Kh. Kaibyshev, Mikhail A. Prosnikov, Peter C. M. Christianen, Aleksei A. Onushchenko, and Manfred Bayer

S1. Absorption spectra

In Figures S1(a-d) we show photoluminescence (PL) and absorption spectra for all studied CdSe NCs measured at $T = 4.2$ K. One can clearly see that with decreasing the NC diameter from 6.1 nm down to 3.3 nm the PL maximum is shifted to higher energies from 2.017 eV up to 2.366 eV. This shift is provided by the quantum confinement effect. A similar behavior is seen for the lowest peak in the absorption spectra, which corresponds to the lowest bright exciton state. Namely, it shifts from 2.039 eV up to 2.455 eV. The absorption spectra demonstrate a clear modulation corresponding to the optical transitions between different energy levels.¹ This can be better seen when the second derivative of the absorption spectrum is plotted,^{1,2} see Figures S1(e) and S1(f). For example, in sample D6.1 (Figure S1(f)) the first absorption peak at 2.039 eV is due to the transition between $1S_{3/2}$ and $1S_e$,³ and the second peak at 2.127 eV can be assigned to the transition between $2S_{3/2}$ and $1S_e$. The length of vertical bars reflects the oscillator strength of the transitions. The parameters of all samples evaluated from the PL and absorption spectra are summarized in Table 1. We also present in Figure S2 a comparison between the absorption and photoluminescence excitation (PLE) spectra for the sample D4.9. As one can see, both spectra show maxima near the calculated quantum size levels of the exciton. In the PLE spectrum, several additional narrow features are observed.

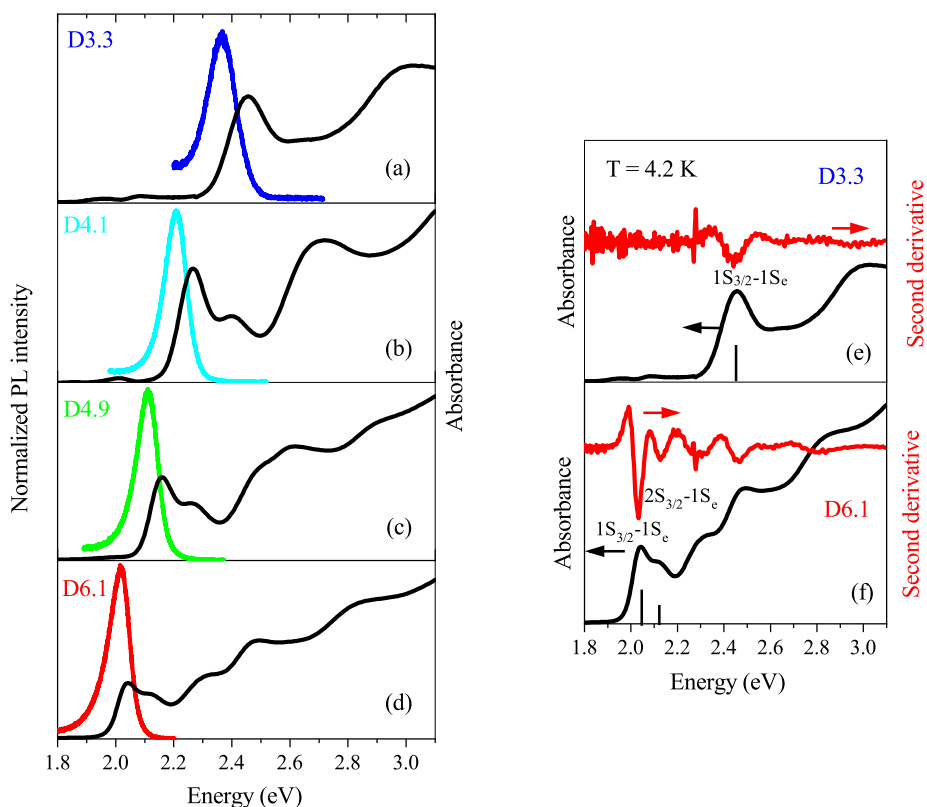


Fig. S1 (a)-(d) PL spectra (color lines) and absorption spectra (black lines) for all studied samples measured at $T = 4.2$ K. (e,f) Absorption spectra (black line) and their second derivatives (red line) for D3.3 and D6.1 samples.

Figure S3 shows the energy of the first absorption maximum as a function of the NC diameter measured by SAXS (see Methods). The results are given for two temperatures of 4.2 and 300 K. At 4.2 K our results are compared with the experimental data from Figure 6 in Ref. 3, obtained at $T = 10$ K for CdSe NCs grown by wet chemistry (blue line).

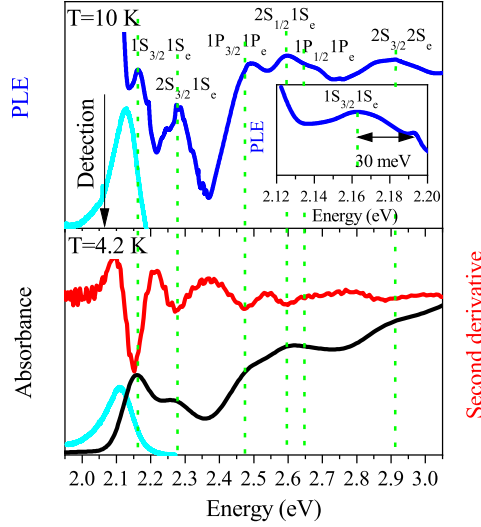


Fig. S2 PLE spectrum at $T = 10$ K and absorption spectrum at $T = 4.2$ K of sample D4.9. Vertical green dashed lines show the quantum size levels of the exciton. The inset shows a narrow feature shifted by 30 meV from the $1S_{3/2}1S_e$ PLE peak. PL spectra measured under nonresonant excitation are shown by the green solid lines.

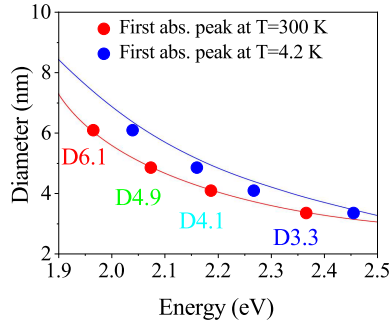


Fig. S3 Exciton absorption energy (the first peak in the absorption spectra) vs NC diameter for the studied CdSe NCs in glass. Symbols are the experimental data points for temperatures of 4.2 K (blue) and 300 K (red). The average NC diameter was determined by SAXS. The red line is an interpolation of the experimental data at $T = 300$ K. The blue line corresponds to the experimental data for the $1S_{3/2}1S_e$ absorption peak at $T = 10$ K for colloidal bare-core CdSe nanocrystals from Figure 6 in Ref. 3

S2. Bright-dark splitting of excitons in CdSe NCs in glass

S2.1 Theory: temperature dependence of recombination dynamics

The exciton fine structure in semiconductor NCs at zero magnetic field is shown schematically in Figure 1(d). If the system is excited by a short laser pulse, the populations of bright and dark excitons are described by the following rate equations:⁴

$$\frac{dN_A}{dt} = -N_A[\Gamma_A + \gamma_0(1 + N_B)] + N_F\gamma_0N_B, \quad (\text{S1})$$

$$\frac{dN_F}{dt} = -N_F(\Gamma_F + \gamma_0N_B) + N_A\gamma_0(1 + N_B). \quad (\text{S2})$$

Here, N_A and N_F are the bright and dark exciton populations, respectively. Γ_A and Γ_F are the radiative recombination rates of the bright and dark excitons. γ_0 is the zero-temperature relaxation rate from the bright $|A\rangle$ to the dark $|F\rangle$ exciton state, it is often referred to as a spin-flip rate. γ_0N_B is the thermal activation rate of the reverse process, where $N_B = 1/[\exp(\Delta E_{AF}/k_B T) - 1]$ is the Bose-Einstein phonon occupation at temperature T . ΔE_{AF} is the bright-dark exciton splitting, k_B is the Boltzmann constant. Under nonresonant excitation, just after the fast initial energy relaxation, the bright and dark exciton states are equally populated: $N_A(t=0) = N_F(t=0)$. To account for the nonradiative recombination, the PL intensity can be written as:

$$I(t) = \eta_A\Gamma_A N_A + \eta_F\Gamma_F N_F, \quad (\text{S3})$$

where η_A and η_F are the radiative quantum efficiencies of the bright and dark states, respectively. By solving the rate equations (S1) - (S3) in the approximation $\gamma_0 \gg \Gamma_A \gg \Gamma_F$, the radiative recombination dynamics reads as:⁴

$$I(t) = \frac{\eta_A \Gamma_A N_B + \eta_F \Gamma_F}{1 + 2N_B} \exp\left(-\frac{t}{\tau_{Long}}\right) + \eta_A \Gamma_A \left[N_A(0) - \frac{N_B}{1 + 2N_B} \right] \exp\left(-\frac{t}{\tau_{Short}}\right), \quad (S4)$$

$$\tau_{Long}^{-1} = \frac{\Gamma_F + \Gamma_A}{2} - \left(\frac{\Gamma_A - \Gamma_F}{2} \right) \tanh\left(\frac{\Delta E_{AF}}{2k_B T}\right), \quad (S5)$$

$$\tau_{Short}^{-1} = \gamma_0(1 + 2N_B). \quad (S6)$$

τ_{Long} and τ_{Short} are the time constants corresponding to the long and short component of the PL decay, respectively. The temperature dependence of the PL decay of excitons in neutral NCs can be described by the equations (S4)-(S6). ΔE_{AF} can be evaluated by fitting an experimentally measured dependence $\tau_{Long}^{-1}(T)$ with equation (S5).

S2.2 Experiment: temperature dependence of PL decay and evaluation of ΔE_{AF}

The photoluminescence dynamics for all studied samples measured at $T = 4.2$ K for $B = 0$ T are shown in Figure S4. The best fits of the PL decays are achieved with four-exponential functions. The fits are shown by the black lines and the corresponding parameters (times and amplitudes) are listed in Table S1. One can see that the characteristic decay times have about the following values: T_1 is on the order of 0.5 ns, T_2 on the order of 3 ns, T_3 on the order of 25 ns, and T_4 on the order of several hundred ns. For colloidal semiconductor NCs, one may expect the bi-exponential decay with the first component related to the bright exciton emission and bright to dark exciton relaxation. The multiexponential decay is the signature of the inhomogeneity in the ensemble where there are nonradiative processes in some of the NCs which accelerate both the bright and dark exciton decays. Similar situation was observed in the Ref. 5, there we also observed multiexponential decay for CdSe nanoplatelets at low temperatures. Corresponding decay were successfully fitted with three exponential function with the long decay component also ascribed to the dark exciton. The intermediate decay component was shown to be related to nonradiative recombination of dark excitons. Probably, in the studied CdSe NCs in the glass these intermediate decay components also correspond to the nonradiative decay of the dark excitons. The shortest time T_1 is also contributed by the bright exciton recombination and its relaxation to the dark exciton state. The longest time T_4 can be assigned to the recombination of dark excitons.

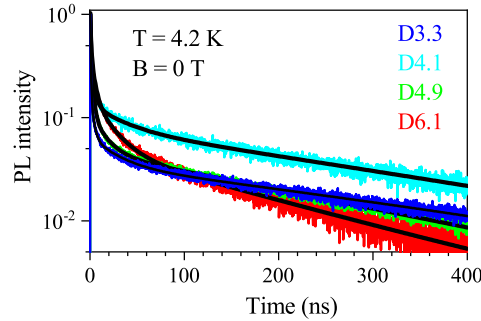


Fig. S4 Photoluminescence decay in CdSe NCs measured at $T = 4.2$ K for $B = 0$ T. The black lines are fits with four-exponential functions.

Table S1 Parameters of the PL decay of the CdSe NCs in glass fitted with four-exponential functions.

Sample	D3.3	D4.1	D4.9	D6.1
NC diameter (nm)	3.3	4.1	4.9	6.1
Time constant T_1 (ns)	0.4	0.5	0.5	0.8
Amplitude A_1	2.1	1.4	1.8	0.9
Time constant T_2 (ns)	2.8	3.3	2.3	4.6
Amplitude A_2	0.2	0.2	0.4	0.3
Time constant T_3 (ns)	27	29	15	23
Amplitude A_3	0.03	0.06	0.07	0.11
Time constant T_4 (ns)	410	315	245	170
Amplitude A_4	0.04	0.08	0.05	0.06

The PL decay can be also reasonably well fitted with three-exponential functions. We show these results for comparison in Figure S5 and give the parameters in Table 1. One can see that the T_1 times are similar in both cases. The T_2 time in the three-exponential fit lies in between the T_2 and T_3 times in the four-exponential fit. The longest T_3 time in the three-exponential fit is about 20 – 25% shorter than the T_4 time in the four-exponential fit. For the evaluation of ΔE_{AF} from the temperature dependence of the longest time, we use

the data from the four-exponential fit.

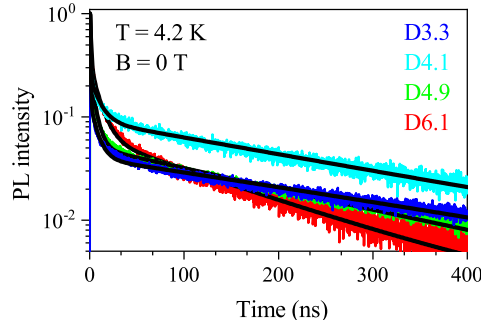


Fig. S5 Photoluminescence decay in CdSe NCs measured at $T = 4.2$ K for $B = 0$ T. The black lines are fits with three-exponential functions.

Table S2 Parameters of the PL decay of CdSe NCs in glass fitted with three-exponential functions.

Sample	D3.3	D4.1	D4.9	D6.1
NC diameter (nm)	3.3	4.1	4.9	6.1
Time constant T_1 (ns)	0.5	0.7	0.6	1.0
Amplitude A_1	2.0	1.3	1.6	1.0
Time constant T_2 (ns)	7.4	9.8	5.7	9.8
Amplitude A_2	0.1	0.2	0.2	0.3
Time constant T_3 (ns)	316	263	208	137
Amplitude A_3	0.04	0.09	0.05	0.06

Figure S6(a) shows a representative example of the PL dynamics variations with increasing temperature from 4.2 up to 50 K. It is given for the sample D4.1 at $B = 0$ T. The long tail of the PL decay shortens with increasing temperature, i.e. the recombination rate τ_{Long}^{-1} accelerates. The temperature dependence of τ_{Long}^{-1} is plotted in Figure S6(b) by dots. The fit by equation (S5) is shown by the red line. From the fit we evaluate the bright-dark splitting $\Delta E_{AF} = 4.3$ meV. The ΔE_{AF} values for the other studied samples are given in Table 1 and shown by the open diamonds in Figure S6(c). They are compared with the literature data available for the wet chemistry grown and glass-embedded CdSe NCs, see the closed circles in Figure S6(c). Good agreement is found for ΔE_{AF} in D6.1, D4.9 and D4.1, while for D3.3, ΔE_{AF} deviates from the general tendency.

Lines in Figure S6(c) show size dependences of ΔE_{AF} calculated as: $\Delta E_{AF} = 2\eta + \Delta/2 - (4\eta^2 + \Delta^2/4 - \eta\Delta)^{1/2}$,^{6,7} where $\eta \propto (a_B/a)^3$ is a measure of the electron-hole exchange interaction, $\Delta = 23$ meV is the crystal field splitting in spherical wurtzite CdSe NCs of the hole states with angular momentum projections $\pm 3/2$ and $\pm 1/2$, $a_B = 5.6$ nm is the exciton Bohr radius in bulk CdSe, a is the NC radius. The dashed line is calculated with accounting for the short-range exchange interaction (but not the long-range) between electron and hole⁶ corresponding to $\eta = 0.1(a_B/a)^3$ meV. The solid line fits ΔE_{AF} determined from FLN (see next section) and it is calculated with $\eta = 0.2(a_B/a)^3$ meV. Note, that the full account of both, short-range exchange and long-range exchange interaction⁷ would correspond to $\eta = 0.37(a_B/a)^3$ meV.

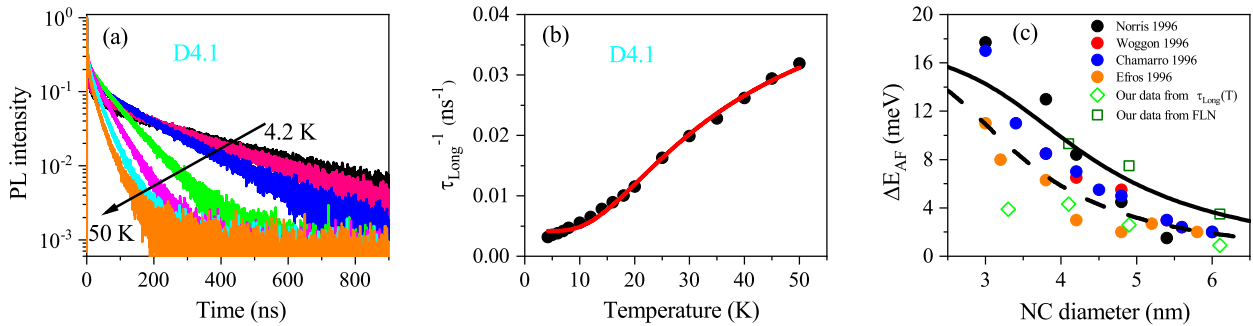


Fig. S6 (a) PL decay in sample D4.1 at various temperatures increasing from 4.2 K up to 50 K. (b) Temperature dependence of the decay rate for the long component τ_{Long}^{-1} in D4.1. The red line shows a fit with equation (S5) for $\Delta E_{AF} = 4.3$ meV. (c) Size dependence of the bright-dark splitting ΔE_{AF} . The green diamonds are the data from $\tau_{Long}(T)$ dependence. The green open squares are the data determined from FLN. Literature data for wet chemistry grown and glass-embedded CdSe NCs are shown by the solid circles.^{6,8-10} Size dependences of ΔE_{AF} calculated with $\eta = 0.1(a_B/a)^3$ meV and $\eta = 0.2(a_B/a)^3$ meV for spherical wurtzite CdSe nanocrystals are shown by dashed and solid lines, respectively.

S2.3 Evaluation of ΔE_{AF} from fluorescence line narrowing

An alternative method of ΔE_{AF} determination is fluorescence line narrowing, which also allows us to compare the intensities of the ZPL and 1PL emission lines of the dark exciton. For resonant excitation of the CdSe NCs we used a ring dye laser with R6G dye and a dye laser with DCM dye. The scattered light was analyzed by a Jobin-Yvon U1000 double monochromator equipped with a cooled GaAs photomultiplier. To record sufficiently strong signals of the dark exciton emission and to suppress the laser stray light, a spectral slit width of 0.2 cm^{-1} (0.025 meV) was used. The measurements were performed on samples immersed in pumped liquid helium (typically at a temperature of 2 K). The FLN signal was measured in backscattering geometry with linearly polarized excitation (H) and subsequent detection of the PL with orthogonal linear polarization (V). We evaluate $\Delta E_{AF} = 3.5, 7.5$ and 8.4 meV in the samples D6.1, D4.9 and D4.1, respectively. The relative intensity of the ZPL emission is larger in nanocrystals with a smaller diameter.

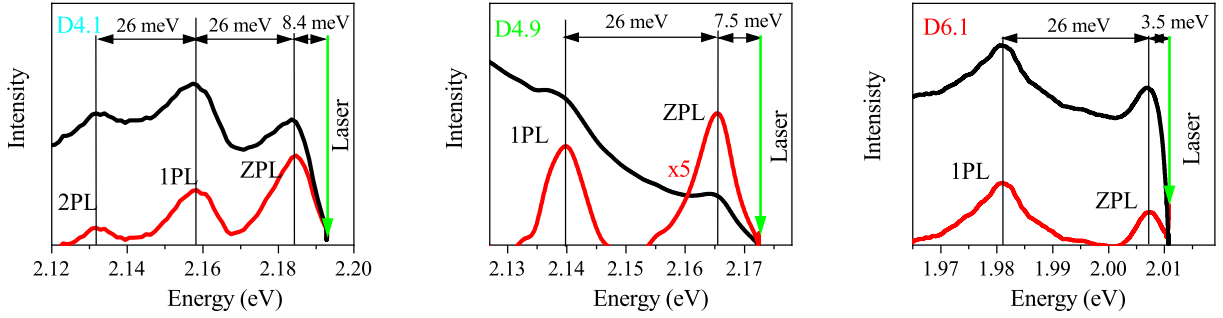


Fig. S7 Fluorescence line narrowing spectra of samples D4.1, D4.9 and D6.1. The black lines show the FLN spectra as recorded. The red lines show the ZPL and 1PL emission after subtraction of the nonresonant PL background. The black arrows show the energies of the optical phonon $E_{LO} = 26 \pm 0.5 \text{ meV}$ and the bright-dark exciton splittings $\Delta E_{AF}(D4.1) = 8.4 \text{ meV}$, $\Delta E_{AF}(D4.9) = 7.5 \text{ meV}$ and $\Delta E_{AF}(D6.1) = 3.5 \text{ meV}$.

S3. Degree of circular polarization (DCP) dynamics

The magnetic field induced circular polarization is determined by the exciton population of the Zeeman spin levels split in a magnetic field. The equilibrium DCP, P_c^{eq} , is determined only by the thermal distribution, i.e. by the ratio of the exciton Zeeman splitting to the thermal energy $k_B T$, while the time-integrated DCP, P_c^{int} , is also affected by the spin-relaxation and recombination processes.¹¹ It is because when the spin relaxation time is longer than the exciton lifetime, the thermal equilibrium is not established, which results in $P_c^{int} < P_c^{eq}$. The relationship between them can be described by $P_c^{int}(B) = d P_c^{eq}(B)$, where $0 < d \leq 1$ is the so-called dynamical factor. In case of a single exponential decay $d = \tau / (\tau + \tau_s)$, where τ is the exciton lifetime and τ_s is the exciton spin relaxation time. For a multi-exponential decay, an averaging should be made, accounting for the times and relative amplitudes of each component, e.g. see Ref. 5. For the present study it is important to ensure that the P_c^{int} measured under cw excitation is close to P_c^{eq} , i.e., that $d \approx 1$.

The polarization-resolved PL decay is shown in Figure S8(a) for the sample D6.1. The σ^- and σ^+ polarized components are measured at $T = 2.2 \text{ K}$ and $B = 17 \text{ T}$, and the corresponding time-resolved DCP $P_c(t)$ is shown by the black line. After pulsed laser excitation, the DCP changes rapidly within a nanosecond from 0 to about -0.35 , and then slowly evolves until saturating at -0.49 , which corresponds to the equilibrium DCP, P_c^{eq} . $P_c(t)$ can be described by the following empirical expression:¹²

$$P_c(B, t) = P_c^{eq}(B)[1 - \exp(-t/\tau_s(B))], \quad (S7)$$

where τ_s characterize the DCP rise time but is not the true spin relaxation time in general case. P_c^{eq} is strongly influenced by the magnetic field and temperature, see Figure S8(b). It increases with increasing magnetic field and is suppressed by elevated temperature. At $T = 2.2 \text{ K}$, P_c^{eq} varies from 0 up to -0.48 at $B = 15 \text{ T}$, when the temperature increases, it drops to -0.44 at $T = 4.2 \text{ K}$ and to -0.38 at $T = 6 \text{ K}$.

Figure S9(a) shows the time-resolved DCP measured at $B = 5 \text{ T}$ for various temperatures, which can be well reproduced by equation (S7), see the solid red lines. With increasing temperature, the DCP rise accelerates, while the equilibrium DCP, P_c^{eq} , decreases (-0.30 at $T = 2.2 \text{ K}$ and -0.08 at $T = 10 \text{ K}$) as shown in Figure S9(b).

Figure S10 shows the magnetic field dependence of P_c^{int} at $T = 20 \text{ K}$ and 4.2 K for comparison. The P_c^{int} at $T = 20 \text{ K}$ is smaller than the one at liquid helium temperature and changes almost linearly with magnetic field.

The magnetic field dependence of the dynamical factor $d(B) = P_c^{int}(B)/P_c^{eq}(B)$ in all studied samples is shown in Figure S11. At $T = 4.2 \text{ K}$ it is close to unity. Therefore, the time-integrated DCP is close to the value expected for the equilibrium exciton polarization.

In Figure S12, we present a comparison of the magnetic field dependences of the time-integrated DCP measured in this work with the dependences from Refs. 13–16. One can see that in all cases a similar increase of the DCP in low magnetic fields is observed, while the saturation of the DCP at $B = 30 \text{ T}$ varies significantly. For glass embedded CdSe NCs the saturation value of the DCP in high magnetic

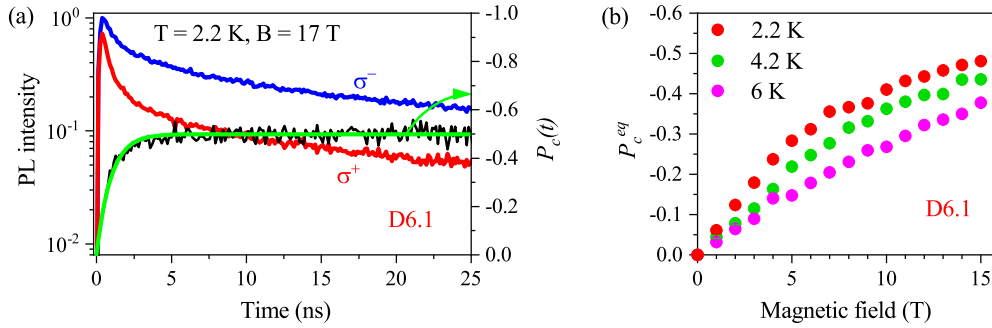


Fig. S8 (a) Polarized PL decay for sample D6.1 measured for $T = 2.2$ K and $B = 17$ T. Red and blue lines correspond to σ^+ and σ^- polarizations, respectively. Black line shows the time-resolved DCP. (b) Magnetic field dependence of equilibrium DCP (P_c^{eq}) at $T = 2.2, 4.2$ and 6 K for the sample D6.1.

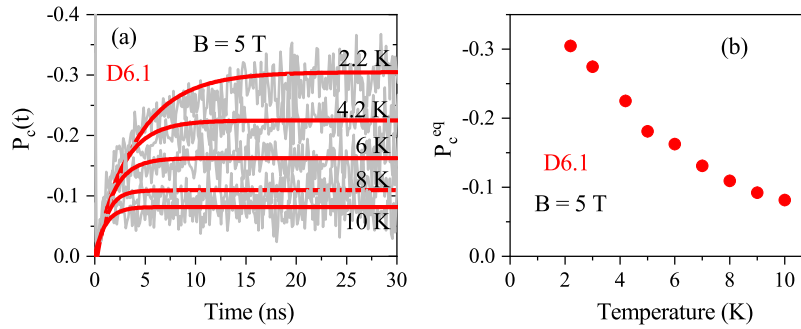


Fig. S9 (a) Temperature dependence of the time-resolved DCP, $P_c(t)$, at $B = 5$ T, shown by grey curves. Red lines are fits with equation (S7). (b) Temperature dependence of the equilibrium DCP, P_c^{eq} , at $B = 5$ T for sample D6.1.

fields increases with decreasing NC diameter. For the colloidal CdSe NCs studied in Refs. 13–16 there is no obvious dependence of the DCP saturation on the NC diameter.

S4. Model description

S4.1 ZPL and 1PL emission

To describe the experimental dependences of the DCP and the positions of the σ^+ and σ^- polarized PL maxima, we extend the theoretical model of the circularly polarized emission from an ensemble of randomly oriented nanocrystals, first developed in Ref. 13. The extension accounts for the linearly polarized contribution coming from the dark exciton recombination assisted by optical phonons. The model in Ref. 13 accounted for only the zero phonon line (ZPL) emission of the ± 2 dark excitons via the admixture of the $\pm 1^L$ bright excitons. This admixture results in the recombination of the ± 2 dark excitons with the emission of photons that are circularly polarized in the plane perpendicular to the c-axis of a nanocrystal (Figure S13).^{6,17} The spatial distribution of the PL intensity, in this

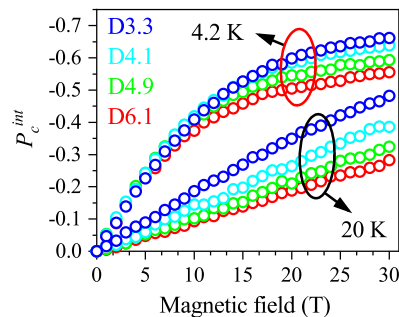


Fig. S10 Magnetic field dependence of the P_c^{int} at $T = 4.2$ K and 20 K for all samples.

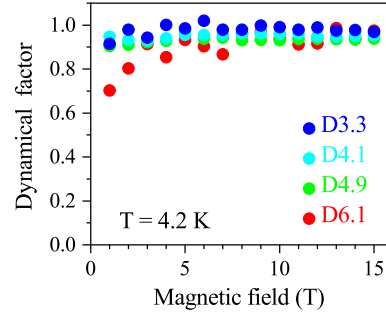


Fig. S11 Magnetic field dependence of the dynamical factor d measured at $T = 4.2$ K.

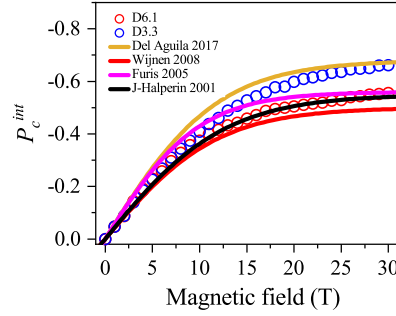


Fig. S12 Magnetic field dependences of the DCP at $T = 4.2$ K in CdSe nanocrystals from the present study (open circles) and literature data: red line from Ref. 15 for 3.6 nm CdSe/CdS(1ML) NCs, black line from Ref. 13 for 5.7 nm CdSe NCs, magenta line from Ref. 14 for 2.6 nm CdSe/ZnS NCs (average between DCP at $T = 1.6$ K and 10 K), yellow line from Ref. 16 for CdSe and CdSe/CdS NCs with diameters of 3.5 – 5 nm.

case, corresponds to the emission of a 2D dipole and has a maximum for the propagation of light along the direction of the c-axis (Figure S13(c)). The model in Ref. 13 does not consider the contribution of the optical phonon-assisted recombination of the dark excitons.

However, it is well known from fluorescence line narrowing experiments, that the dark exciton PL also has a strong contribution from optical phonon-assisted recombination.^{8,9} In the model described below, we consider the recombination of dark excitons with the assistance of one optical phonon, the so-called 1PL emission. The 1PL emission is arranged predominantly via admixture of the 0^U bright exciton.¹⁷ This results in the recombination of ± 2 dark excitons with the emission of photons that are linearly polarized along the c-axis of a nanocrystal.^{6,17} The spatial distribution of the PL intensity, in this case, corresponds to the emission of the 1D dipole and has a maximum for the propagation of light in the plane perpendicular to the c-axis (Figure S13(c), green curve). Also, we analyze the impact of the dark exciton recombination via the admixture of the 0^U bright exciton, caused by the interaction with acoustic phonons.¹⁷ The inhomogeneous broadening of the PL spectra in the samples under investigation is much larger than the typical energies of the acoustic phonons. For this reason, we neglect the energy shift between the ZPL emission and the acoustic phonon-assisted emission, i.e. we consider the emission at the ZPL energy which includes the contributions coming from the admixture of the 0^U and $\pm 1^L$ bright excitons to the dark exciton.

With the account of the ZPL and 1PL contributions and the random orientation of the NCs in an ensemble, the spectral dependences of the σ^\pm polarized PL intensities in a magnetic field are given by:

$$I^\pm(E, B) = \int_0^1 dx \sum_{i=\pm 2} \left[I_{i,ZPL}^\pm(x, B) f_{ZPL}(E - \delta E_i(B, x)) + I_{i,1PL}^\pm(x, B) f_{1PL}(E - \delta E_i(B, x)) \right], \quad (\text{S8})$$

where $\delta E_{\pm 2}(B, x) = \pm g_F \mu_B B x / 2$ are the Zeeman shifts of the ± 2 dark excitons, μ_B is the Bohr magneton, g_F is the dark exciton g -factor, $x = \cos \theta$ with θ being the angle between the c-axis of the nanocrystal and the magnetic field direction. $I_{i,ZPL}^\pm(x, B)$ and $I_{i,1PL}^\pm(x, B)$ are the intensities of the dark exciton emission with σ^+ (σ^-) polarization in the external magnetic field applied in the Faraday geometry for NCs without and with emission of an optical phonon, respectively.

The functions $f_{ZPL}(E)$ and $f_{1PL}(E)$ determine the inhomogeneous broadening of the PL spectra due to the NC size dispersion in an

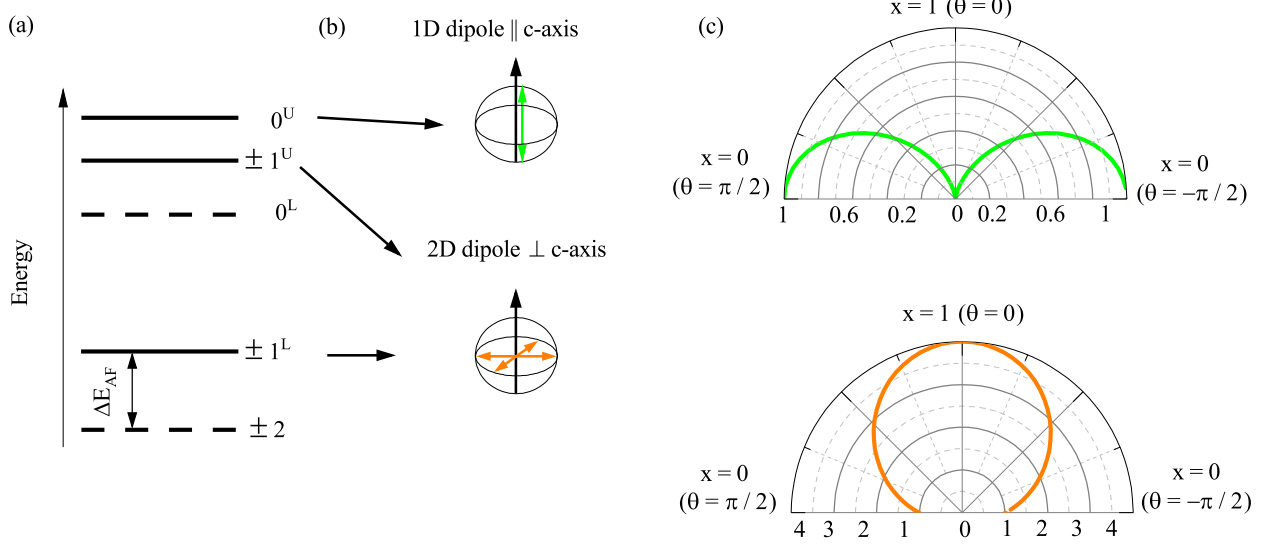


Fig. S13 (a) Fine structure of the $1S_{3/2}1S_e$ exciton. Dashed lines show the dark excitons ± 2 and 0^L . Solid lines show the bright excitons $\pm 1^L$, $\pm 1^U$ and 0^U . (b) The emission of the 0^U bright exciton has the properties of a 1D dipole, while the emission of the $\pm 1^L$ and $\pm 1^U$ bright excitons has the properties of a 2D dipole. (c) Spatial distribution of the emission intensity for the $\pm 1^L$, $\pm 1^U$ excitons (orange line) and the 0^U exciton (green line) with respect to the direction of the c -axis.⁶

ensemble. We consider the case of a normal distribution:

$$f_{ZPL}(E - \delta E_i(B, x)) = \frac{1}{w\sqrt{2\pi}} \exp\left(-\frac{(E - \delta E_i(B, x) - E_{ZPL}^0)^2}{2w^2}\right), \quad (\text{S9})$$

$$f_{1PL}(E - \delta E_i(B, x)) = \frac{1}{w\sqrt{2\pi}} \exp\left(-\frac{(E - \delta E_i(B, x) - E_{1PL}^0)^2}{2w^2}\right) = f_{ZPL}(E - \delta E_i(B, x) + E_{LO}).$$

Here $E_{LO} = 26$ meV is the optical phonon energy in CdSe, E_{ZPL}^0 and $E_{1PL}^0 = E_{ZPL}^0 - E_{LO}$ are the maxima of the ZPL and 1PL emission from the dark excitons, corresponding to the maximum of the size distribution.

The experimental data on the DCP of the emission presented in this paper are measured under continuous-wave excitation. Thus, we are interested in the time-integrated PL intensities $I_{i,ZPL}^\pm(x, B)$ and $I_{i,1PL}^\pm(x, B)$, which are defined as follows:

$$I_{\pm 2, ZPL}^\pm(x, B) = \Gamma_{\pm 2, ZPL}^\pm(x, B) N_{ex}(x, B), \quad I_{\pm 2, 1PL}^\pm(x, B) = \Gamma_{\pm 2, 1PL}^\pm(x, B) N_{ex}(x, B), \quad (\text{S10})$$

$$N_{ex}(x, B) = \frac{G}{\gamma_{tot}(x, B)}, \quad (\text{S11})$$

where G is the generation rate of excitons, γ_{tot} is the total exciton recombination rate, N_{ex} is the equilibrium population of the excitons.

The external magnetic field not only splits the exciton Zeeman sublevels (by the field component parallel to the c -axis), but also mixes the bright to the dark exciton states (by the field component perpendicular to the c -axis). This mixing results in the additional activation of the dark exciton, which can be described within second order perturbation theory in moderate magnetic fields^{6,17}. The resulting magnetic field and angular dependent recombination rates $\Gamma_{\pm 2, ZPL}^\pm(x, B)$ contributing to the ZPL emission are given by:

$$\Gamma_{-2, ZPL}^\pm(x, B) = \frac{1}{2} \gamma_{\epsilon n-2}(x, B) \left[\left(\left(\frac{g\epsilon \mu_B B}{2\sqrt{2}\epsilon} \right)^2 (1-x^2) + 1 \right) (1 \mp x)^2 + \chi_{ac}(1-x^2) \right], \quad (\text{S12})$$

$$\Gamma_{+2, ZPL}^\pm(x, B) = \frac{1}{2} \gamma_{\epsilon n+2}(x, B) \left[\left(\left(\frac{g\epsilon \mu_B B}{2\sqrt{2}\epsilon} \right)^2 (1-x^2) + 1 \right) (1 \pm x)^2 + \chi_{ac}(1-x^2) \right], \quad (\text{S13})$$

$$\gamma_{\epsilon} = \frac{\epsilon^2}{6\eta^2} \frac{1}{\tau_0}, \quad \eta = 0.2 \left(\frac{aB}{a} \right)^3 \text{ meV}. \quad (\text{S14})$$

where g_e is the electron g -factor, ε is the characteristic energy of interaction, which results in the admixture to the dark states of the $\pm 1^L$ bright exciton states in zero magnetic field, $\chi_{ac} = \gamma_{ac}/\gamma_\varepsilon$ is the ratio of the linearly and circularly polarized recombination rates of the ZPL emission at $B = 0$ T, τ_0 is the lifetime of the 0^U bright exciton, $n_{\pm 2}(x, B)$ are the Boltzmann populations of the ± 2 dark exciton states, respectively. Note that the angular dependence (x -dependence) arises not only from the perpendicular component of the magnetic field, but is also caused by the spatial profiles of the emission distribution for the 1D and 2D dipoles. In modeling we use $\eta = 0.2(a_B/a)^3$ meV which fits ΔE_{AF} values from FLN measurements. The only parameter in our modeling which depends on η is r_{lin} determining polarization properties of 1PL emission (see below). For $\eta = 0.1(a_B/a)^3$ meV corresponding to short-range exchange interaction between electron and hole, relative change of r_{lin} does not exceed 2% for the whole range of considered NC diameters, and does not affect our conclusions about the role of the 1PL emission of the dark excitons.

The angle-specific recombination rates of the dark excitons with assistance of the optical phonons are given by:

$$\Gamma_{-2,1PL}^\pm(x, B) = \frac{1}{2} \gamma_\varepsilon \chi(x, B) n_{-2}(x, B) \left[r_{lin}(1-x^2) + (1-r_{lin})(1 \mp x)^2 \right], \quad (S15)$$

$$\Gamma_{+2,1PL}^\pm(x, B) = \frac{1}{2} \gamma_\varepsilon \chi(x, B) n_{+2}(x, B) \left[r_{lin}(1-x^2) + (1-r_{lin})(1 \pm x)^2 \right], \quad (S16)$$

$$\chi(x, B) = \chi_0 \left[1 + c_{1PL} \left(\frac{g_e \mu_B B}{2\sqrt{2}\varepsilon} \right)^2 (1-x^2) \right]. \quad (S17)$$

Here $\chi_0 = \gamma_{LO}/\gamma_\varepsilon$ is the ratio of the 1PL recombination rate to the ZPL recombination rate at $B = 0$ T. c_{1PL} is a phenomenological parameter, which determines the increase of the 1PL recombination rate in a magnetic field. The parameter r_{lin} determines the fraction of the optical phonon-assisted recombination rate via the admixture to the 0^U bright exciton. According to Ref. 17 it equals to:

$$r_{lin} = \left(\frac{E_{LO}^2 (\Delta + 4\eta + E_{LO})^2}{2(3\Delta\eta + E_{LO}(\Delta + 4\eta) + E_{LO}^2) + 1} \right)^{-1}. \quad (S18)$$

The factor 2 in the denominator instead of 4 in equation (19) from Ref. 17 is used because here we are interested in recombination rates, while in Ref. 17 transition dipole moments were compared.

The total recombination rate equals to:

$$\gamma_{tot}(x, B) = \gamma_\varepsilon \left[\left(\frac{g_e \mu_B B}{2\sqrt{2}\varepsilon} \right)^2 (1-x)^2 + 1 + \chi(x, B) + \chi_{ac} \right]. \quad (S19)$$

S4.2 Ensemble-averaged PL decay

The fitting of the DCP and the positions of the polarized PL maxima is performed together with fitting of the $\tau_{Long}(B)$ dependence. As the PL decay is measured from an ensemble of randomly oriented nanocrystals, we need to develop a procedure for averaging the exciton lifetime over the ensemble. Let us consider the decay of the normalized PL intensity of the dark excitons at a fixed energy E for the randomly oriented ensemble. The increase of the dark exciton recombination rate depends on the angle θ between the c -axis of the NC and the direction of the magnetic field. The total PL decay equals to the sum of decays from NCs having all possible values of the angle θ :

$$I(E, B, t) = A_L \frac{\int_0^1 dx G(x, B) \exp[-t\tilde{\gamma}_{tot}(x, B)]}{\int_0^1 dx G(x, 0)}, \quad (S20)$$

$$\tilde{\gamma}_{tot}(x, B) = \frac{\gamma_{tot}(x, B)}{\gamma_{tot}(x, 0)\tau_{B=0}} = \frac{\gamma_{tot}(x, B)}{(\gamma_\varepsilon + \gamma_{LO} + \gamma_{ac})\tau_{B=0}}, \quad (S21)$$

$$G(x, B) = f_{ZPL}(E) \sum_{i=\pm 2} \Gamma_{i,ZPL}^\pm(x, B) + f_{1PL}(E) \sum_{i=\pm 2} \Gamma_{i,1PL}^\pm(x, B). \quad (S22)$$

Here $I(E, B, 0)$ is PL intensity at $t = 0$, A_L is the amplitude of the decay component corresponding to the dark exciton recombination in the total PL decay. Note that $\gamma_{tot}(x, 0) = \gamma_\varepsilon + \gamma_{LO} + \gamma_{ac}$ is the radiative recombination rate of the dark excitons in zero magnetic field and $\tau_{B=0}$ is the lifetime of the dark excitons in zero magnetic field. We neglected the contribution of the Zeeman splitting of the dark excitons in the functions $f_{ZPL}(E)$ and $f_{1PL}(E)$, as these energies are much smaller than the characteristic PL linewidth. The characteristic lifetime determining the PL decay of the dark excitons in magnetic field for a randomly oriented ensemble of NCs can be calculated as:

$$\tau_{ens}(B) = \frac{\int_0^1 dx G(x, B) \tilde{\gamma}_{tot}(x, B)^{-1}}{\int_0^1 dx G(x, B)}. \quad (S23)$$

It has the meaning of an ensemble-averaged dark exciton lifetime. The comparison of the calculated lifetimes $\tau_{\text{ens}}(B)$ (curves) and the experimental times $\tau_{\text{Long}}(B)$ (symbols) is presented in Figure 1(f). The fitting parameters are ε , χ_0 , χ_{ac} , and c_{1PL} , see Tables S3 and S4. These parameters are fixed by fitting the $\tau_{\text{Long}}(B)$ dependences and used in the further fitting of the field dependences of the PL intensities and PL maxima.

S4.3 Energy of PL maximum in zero magnetic field

In an inhomogeneous ensemble of NCs the energy of the PL maximum at $B = 0$ T is determined by the relative intensities of the ZPL and 1PL emission of the dark excitons. One can find the energy of the PL maximum using the following consideration. At $B = 0$ T the PL intensity is given by:

$$I^{\pm}(E) = \int_0^1 dx \sum_{i=\pm 2} \left[I_{i,ZPL}^{\pm}(x) f_{ZPL}(E) + I_{i,1PL}^{\pm}(x) f_{1PL}(E) \right]. \quad (\text{S24})$$

In zero magnetic field the averaging over the random angle distribution of the ensemble in Eq. (S24) results in the same intensity for both circular polarizations $I^+(E) = I^-(E)$, as expected.

We can rewrite Eq. (S24) in zero magnetic field as

$$I^{\pm}(E, 0) = f_{ZPL}(E) \langle I_{ZPL} \rangle + f_{1PL}(E) \langle I_{1PL} \rangle, \quad (\text{S25})$$

where

$$\langle I_{ZPL} \rangle = \int_0^1 dx \sum_{i=\pm 2} I_{i,ZPL}^{\pm}(x, 0) = \frac{4 + 2\chi_{ac}}{3(1 + \chi_0)}, \quad (\text{S26})$$

$$\langle I_{1PL} \rangle = \int_0^1 dx \sum_{i=\pm 2} I_{i,1PL}^{\pm}(x, 0) = \frac{2\chi_0(2 - r_{\text{lin}})}{3(1 + \chi_0)}. \quad (\text{S27})$$

Taking the derivative of Eq. (S25) we find the following condition for the PL maximum E_{max} as

$$E_{\text{max}} = E_{ZPL}^0 - \frac{E_{LO}}{1 + \beta_0 f(E_{\text{max}})} = E_{ZPL}^0 - E_{LO} \tilde{\beta}_0(E_{\text{max}}), \quad (\text{S28})$$

where $\beta_0 = \langle I_{ZPL} \rangle / \langle I_{1PL} \rangle = (2 + \chi_{ac}) / \chi_0(2 - r_{\text{lin}})$, $\tilde{\beta}_0 = (1 + \beta_0 f(E_{\text{max}}))^{-1}$ and

$$f(E_{\text{max}}) = \frac{f_{ZPL}(E_{\text{max}})}{f_{1PL}(E_{\text{max}})} = \exp \left[\frac{E_{LO}^2 (1 - 2\tilde{\beta}_0(E_{\text{max}}))}{2w^2} \right]. \quad (\text{S29})$$

It should be noted that the parameter β_0 allows us to find the relation between χ_{ac} and χ_0 in zero magnetic field. The parameter β_0 can be determined from the comparison of the ZPL and 1PL intensities measured in fluorescence line narrowing experiments.

In Figure S14(a) the dependence of E_{max} on the parameter χ_0 is presented with $\chi_{ac} = 0$, $r_{\text{lin}} = 0.7$ and $w = 30$ meV. One can see that an increase of χ_0 , representing the relative intensity of the 1PL emission, results in a shift of E_{max} towards the maximum of the 1PL emission. For a fixed $\chi_0 = 1.5$ one can see in Figure S14(b) that a sufficiently large inhomogeneous broadening ($w > 15$ meV) results in a constant shift of E_{max} from E_{ZPL}^0 . For $w < 15$ meV a sharp return of E_{max} to E_{ZPL}^0 is observed. The reason is that the spectra of the ZPL and 1PL emission do not overlap anymore. In this case one can separate the ZPL and 1PL peaks, as usually observed in fluorescence line narrowing experiments.

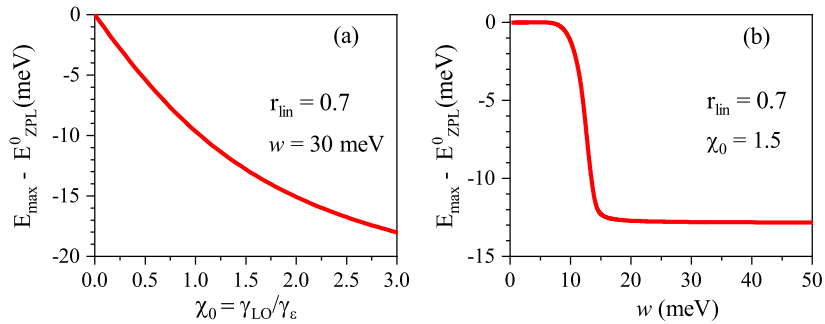


Fig. S14 Energy of the PL maximum E_{max} as a function of (a) the LO-assisted recombination rate and (b) the inhomogeneous broadening of PL spectrum.

S4.4 Calculation of PL maximum energy in magnetic field

To calculate the energies of the σ^+ and σ^- polarized PL maxima, presented in Figures 3(e-h), we use the following approach. Taking the derivative of Eq. (S8), we find a condition for the total maxima of the σ^\pm polarized PL in magnetic field, $E_{\max}^\pm(B)$. We assume that the Zeeman energies δE_i and the maximum shifts in magnetic field $\Delta E_{\max}^\pm(B) = E_{\max}^\pm(B) - E_{\max}$ are much smaller than w and keep only the linear-in-magnetic field corrections to the energy terms and to the distribution functions, to write the following conditions for $\Delta E_{\max}^\pm(B)$:

$$\begin{aligned} \Delta E_{\max}^\pm(B) &= \frac{g_F \mu_B B}{2} \frac{\langle \delta I_{ZPL}^\pm(B) \rangle f_0 (1 - E_{LO}^2 \tilde{\beta}_0^2 / w^2) + \langle \delta I_{1PL}^\pm(B) \rangle [1 - E_{LO}^2 (1 - \tilde{\beta}_0)^2 / w^2]}{\langle I_{ZPL}^\pm(B) \rangle f_0 (1 - E_{LO}^2 \tilde{\beta}_0^2 / w^2) + \langle I_{1PL}^\pm(B) \rangle [1 - E_{LO}^2 (1 - \tilde{\beta}_0)^2 / w^2]} \\ &+ E_{LO} \frac{\tilde{\beta}_0 (f_0 \beta_\pm(B) + 1) - 1}{f_0 \beta_\pm(B) (1 - E_{LO}^2 \tilde{\beta}_0^2 / w^2) + [1 - E_{LO}^2 (1 - \tilde{\beta}_0)^2 / w^2]}. \end{aligned} \quad (S30)$$

Here,

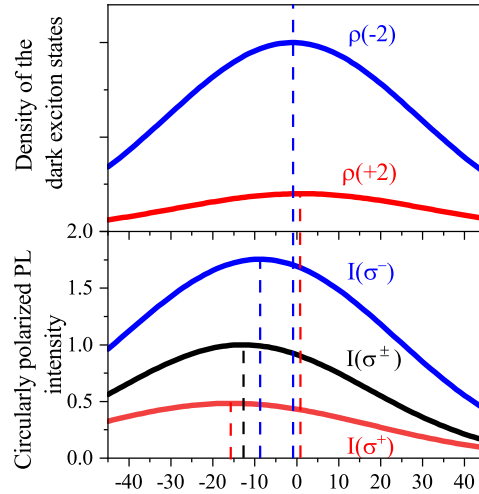
$$\langle I_{ZPL}^\pm(B) \rangle = \int_0^1 dx \sum_{i=\pm 2} I_{i,ZPL}^\pm(x, B), \quad \langle I_{1PL}^\pm(B) \rangle = \int_0^1 dx \sum_{i=\pm 2} I_{i,1PL}^\pm(x, B), \quad (S31)$$

$$\langle \delta I_{ZPL}^\pm(B) \rangle = \int_0^1 dx [I_{+2,ZPL}^\pm(x, B) - I_{-2,ZPL}^\pm(x, B)], \quad (S32)$$

$$\langle \delta I_{1PL}^\pm(B) \rangle = \int_0^1 dx [I_{+2,1PL}^\pm(x, B) - I_{-2,1PL}^\pm(x, B)], \quad (S33)$$

and $\beta_\pm(B) = \langle I_{ZPL}^\pm(B) \rangle / \langle I_{1PL}^\pm(B) \rangle$. The second term in Eq. (S30) depends on the magnetic field only via $\beta_\pm(B)$. Note that $\beta_\pm(0) = \beta_0$ and both terms in Eq. (S30) vanish at $B = 0$.

Schematic in Figure S15 shows the density of dark exciton states ± 2 split in magnetic field (upper panel) for the ensemble of nanocrystals with size dispersion $\sim 5\%$. The energy of the -2 state is lower, and its population (density) is higher. When we consider both ZPL and 1PL emission of the dark excitons (lower panel), we find that left- and right-handed polarized PL maxima are shifted to lower energies as compared to the maxima of -2 and +2 densities of states in the upper panel. Wherein the maximum of σ^- PL spectrum has higher energy, and its intensity is also higher.



Energy with respect to the dark exciton energy E_{ZPL}^0 at $B=0T$ in nanocrystals with diameter corresponding to the maximum of size distribution (meV)

Fig. S15 Density of the dark exciton states ± 2 (upper panel) and spectra of the circularly polarized PL (lower panel). Blue and red curves are plotted for $B=30T$. The black curve shows PL spectra at $B=0T$. Vertical dash lines show maxima positions. Spectra are plotted for a randomly oriented ensemble of nanocrystals with accounting for size dispersion.

S4.5 Fitting parameters

The calculated results presented in Figures 1f, 2 and 3 were achieved assuming that the ZPL emission is governed solely by the admixture of the $\pm 1^L$ bright exciton. The fit parameters for this scenario are given in Table S3.

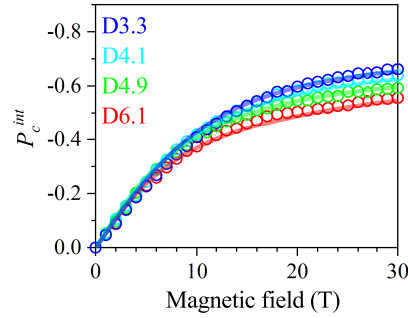
Table S3 Fitting parameters in Figures 1f, 2 and 3.

Sample	D3.3	D4.1	D4.9	D6.1	
g_F	1.6	1.8	1.8	1.6	best fit
g_e	1.42	1.32	1.23	1.1	Refs. 18–20
g_h	-0.06	-0.16	-0.19	-0.16	$g_h = (g_e - g_F)/3$
ε (meV)	0.23	0.24	0.25	0.32	best fit
$\chi_0 = \gamma_{LO}/\gamma_e$	0.8	1	1.3	1.5	best fit
$\chi_{ac} = \gamma_{ac}/\gamma_e$	0	0	0	0	
c_{1PL}	0.2	0.35	0.45	0.5	best fit
w (meV)	50	36	32	30	PL linewidth

We also considered the case, in which the ZPL emission contains a contribution from the recombination of the dark excitons via the admixture of the 0^U bright exciton. For all studied samples we assumed that the recombination rates of the dark excitons through the admixture of the $\pm 1^L$ and 0^U bright excitons are equal, i.e. $\chi_{ac} = \gamma_{ac}/\gamma_e = 1$. The fit results in this case are presented in Figures S16 and S17. Within this scenario we also observe a good agreement with the experimental data. The main result that we obtain from the inclusion of the dark exciton recombination via the admixture of the 0^U bright exciton is an increase of the g -factor $g_F \approx 2.5$ which is close to the value reported for single CdSe NCs.²¹ The dark exciton g -factors and other fitting parameters for this scenario are given in Table S4.

Table S4 Fitting parameters in Figures S16, S17 and S19.

Sample	D3.3	D4.1	D4.9	D6.1	
g_F	2.4	2.6	2.6	2.4	best fit
g_e	1.42	1.32	1.23	1.1	Refs. 18–20
g_h	-0.32	-0.42	-0.45	-0.43	$g_h = (g_e - g_F)/3$
ε (meV)	0.18	0.19	0.19	0.25	best fit
$\chi_0 = \gamma_{LO}/\gamma_e$	1	1.4	1.75	2.25	best fit
$\chi_{ac} = \gamma_{ac}/\gamma_e$	1	1	1	1	
c_{1PL}	0.12	0.18	0.25	0.25	best fit
w (meV)	50	36	32	30	PL linewidth

**Fig. S16** Magnetic field dependences of $P_c^{int}(B)$ measured at the PL maximum in all samples under study. Lines are fits with Eq. 3. The contribution to the ZPL emission via admixture of the 0^U bright exciton is taken into account.

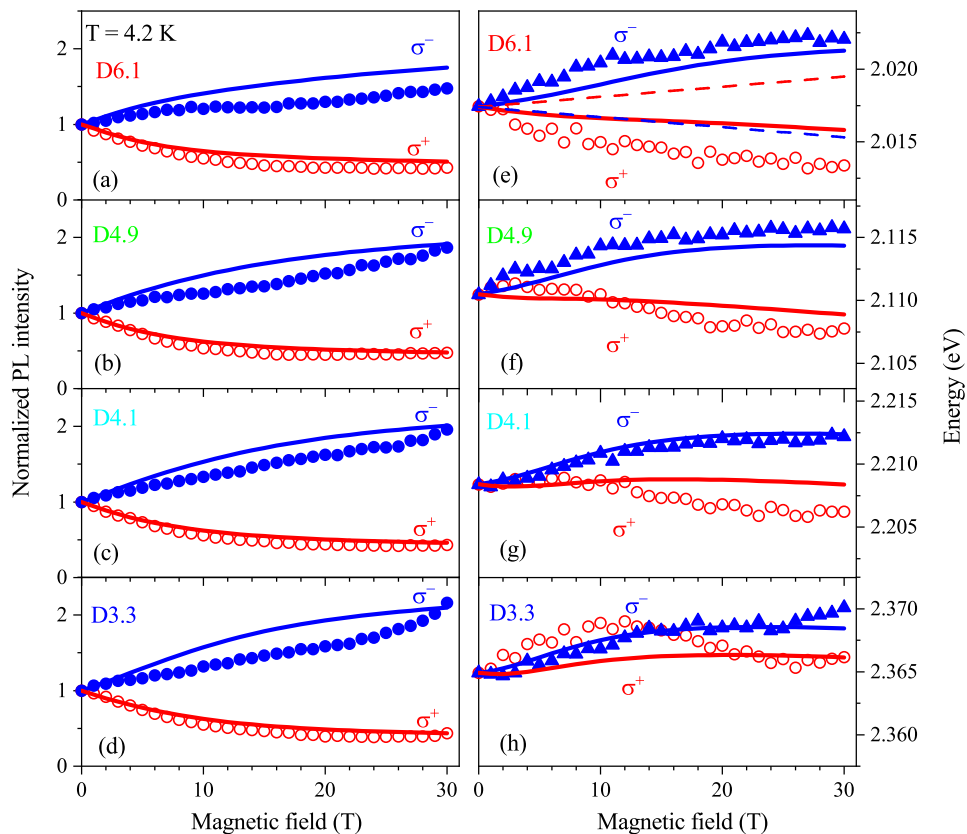


Fig. S17 PL intensity and spectral shifts in magnetic field. (a-d) Time-integrated intensity of the σ^+ (red) and σ^- (blue) polarized PL as function of the magnetic field in CdSe NCs. (e-h) Corresponding PL peak energies. For all panels, the symbols correspond to the experimental data, while curves show the results of calculations. In the calculations, the contribution to the ZPL emission via the admixture of the 0^U bright exciton is taken into account. Dashed lines in panel (e) show the Zeeman splitting of the dark exciton spin sublevels -2 (blue) and $+2$ (red) in a nanocrystal with c-axis parallel to the magnetic field direction and $g_F = 2.4$.

S4.6 Spectral dependence of DCP at $B = 30$ T

Here we present a comparison of the calculated and experimental spectral dependences of the DCP for all studied CdSe NCs at $B = 30$ T. The results of the calculation for the ZPL emission governed only by the admixture of the bright exciton $\pm 1^L$ with the fitting parameters from Table S3 are presented in Figure S18. The results of the calculation with additional inclusion of the ZPL emission governed by the admixture of the bright exciton 0^U with the fitting parameters from Table S4 are presented in Figure S19. From the fit results we conclude that the increase of the degree of the PL polarization towards higher energies is governed by the decrease of the 1PL contribution. This effect is pronounced in large NCs, while in the sample D3.3 the DCP is almost constant across the PL spectrum.

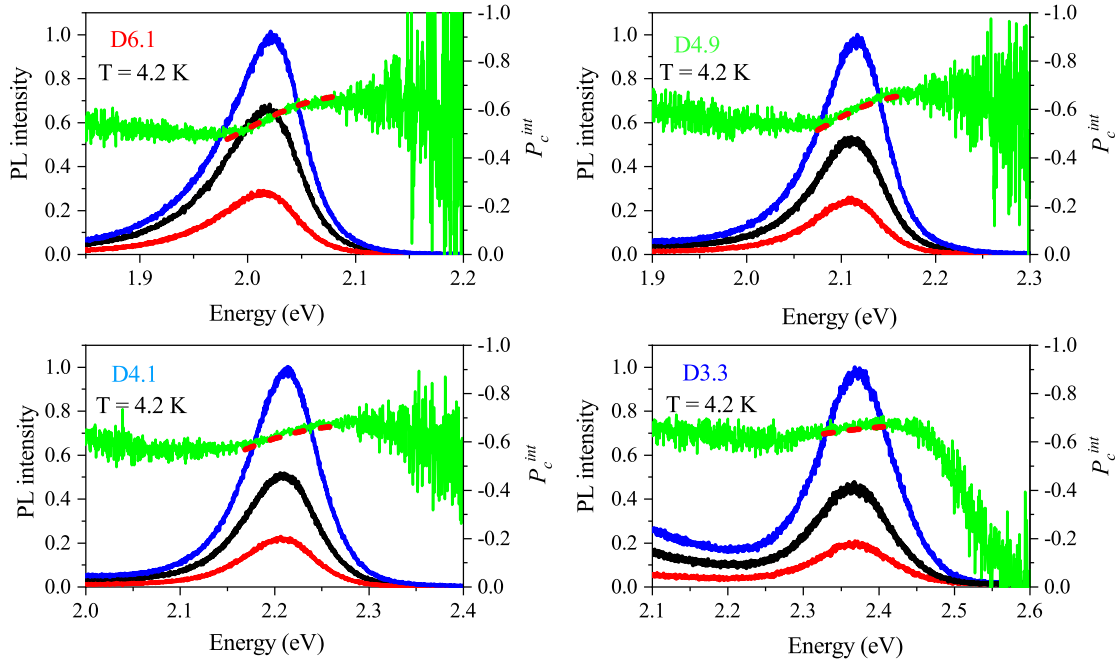


Fig. S18 PL spectra of the σ^+ (red) and σ^- (blue) polarized components at $B = 30$ T and PL spectrum at $B = 0$ T (black). Green line shows the experimental spectral dependence of the circular polarization degree at $B = 30$ T. Red dashed line shows the calculated spectral dependence of the DCP at $B = 30$ T with accounting for the ZPL emission via the admixture of the $\pm 1^L$ bright excitons solely.

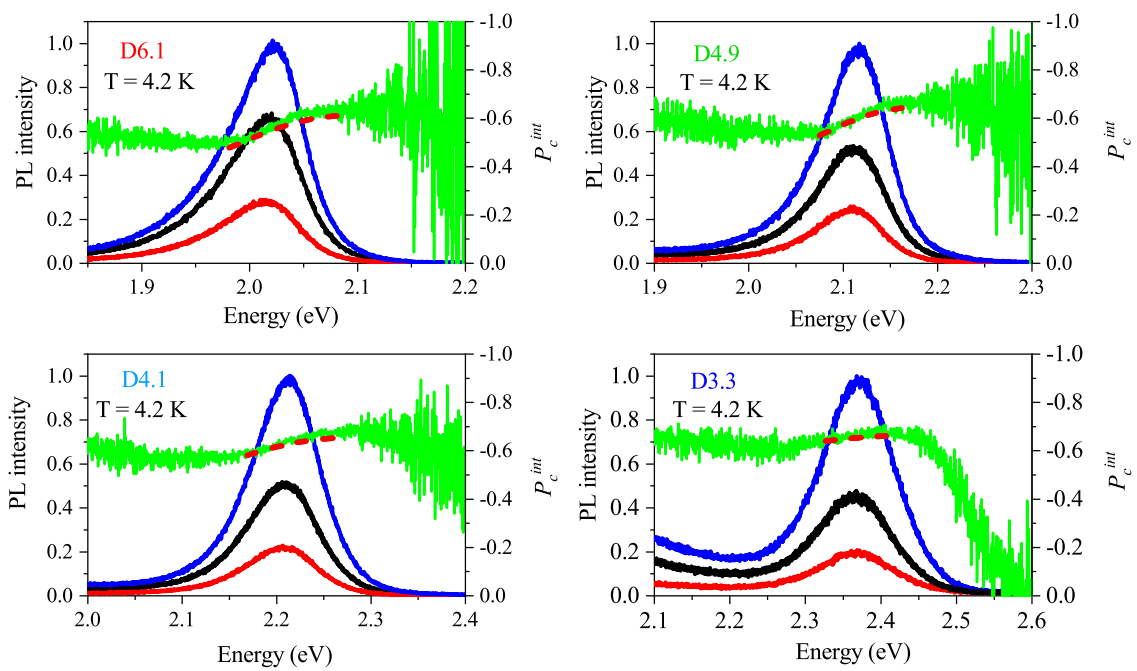


Fig. S19 PL spectra of the σ^+ (red) and σ^- (blue) polarized components at $B = 30$ T and PL spectrum at $B = 0$ T (black). Green line shows the experimental spectral dependence of the circular polarization degree at $B = 30$ T. Red dash line shows the calculated spectral dependence of the DCP at $B = 30$ T. The emission of the dark excitons at the ZPL energy via the admixture of the 0^U bright exciton is included.

S4.7 Fitting for non-equilibrium population of ± 2 states

Here we consider the case when the populations of the ± 2 states due to slow spin relaxation do not approach the equilibrium values in the applied magnetic field. We assume that after nonresonant excitation the excitons relax to the $\pm 1^L$ states which are split in the applied magnetic field. We also assume that before the relaxation to the ± 2 states thermal equilibrium between the $\pm 1^L$ states is achieved. Then excitons from the -1^L state relax to the -2 state, while excitons from the $+1^L$ state relax to the $+2$ state. In this case, the populations of excitons in the ± 2 states are determined by the g -factor of the bright exciton, while the splitting of the ± 2 states is determined by the g -factor of the dark exciton. The relationship between the bright exciton g -factor and the g -factors of electron and hole is given in Ref. 22. From fitting of the experimental data (Figures S20, S21, S22) without the acoustic phonon-assisted contribution to the ZPL, we find $g_h = -0.5$ for D6.1; -0.6 for D4.9; -0.77 for D4.1; and -0.43 for D3.3, with all the other fitting parameters being the same as in Table S3.

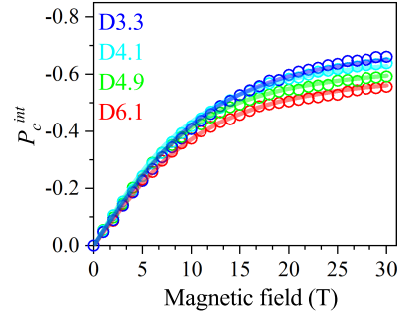


Fig. S20 Magnetic field dependences of the $P_c^{int}(B)$ measured at the PL maximum for all samples. Lines are fits with Eq. 3. Only the contribution to the ZPL emission via the admixture of the $\pm 1^L$ bright exciton is taken into account. The populations of the dark exciton states ± 2 are considered to be determined by the relaxation from the $\pm 1^L$ states.

Considering the acoustic phonon-assisted recombination of the dark excitons in addition to the assumption about the slow spin relaxation between the ± 2 states, we perform fits of the experimental data (Figures S23, S24, S25) with $g_h = -1.2$ for D6.1; -1.4 for D4.9; -1.6 for D4.1; and -1.6 for D3.3. The other fit parameters given in Table S4 remain unchanged, except for $c_{1PL} = 0.08$ for the sample D3.3.

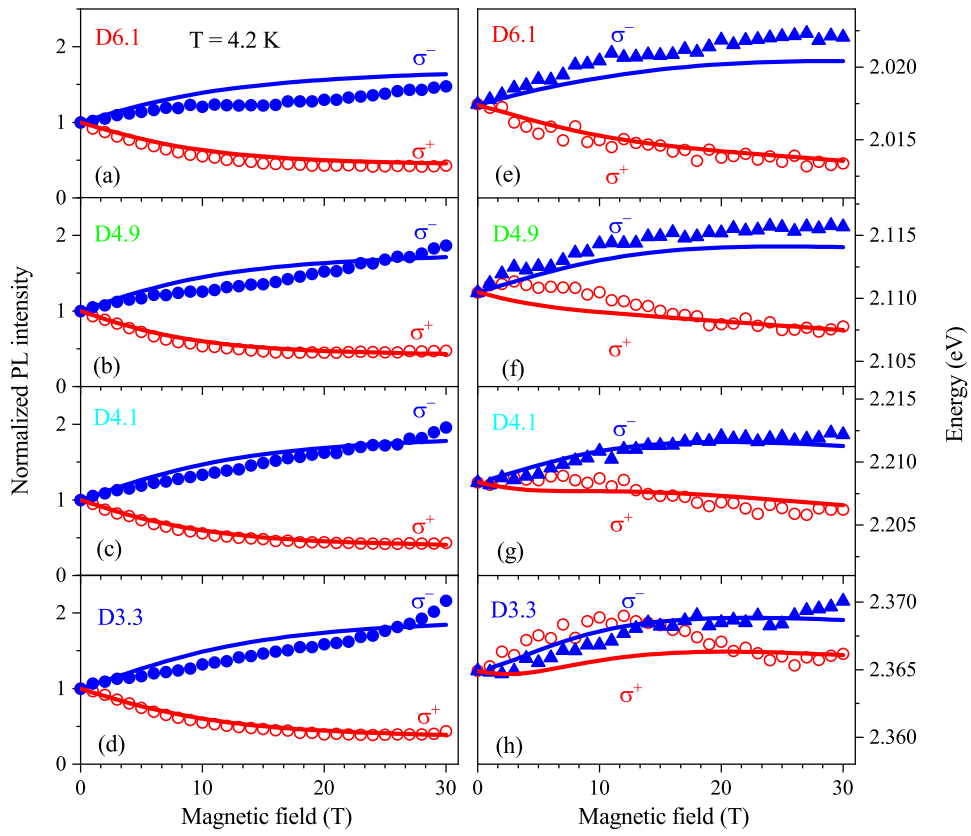


Fig. S21 PL intensity and spectral shifts in magnetic field. (a-d) Time-integrated intensity of the σ^+ (red) and σ^- (blue) polarized PL as function of the magnetic field in CdSe NCs. (e-h) Magnetic field dependences of the corresponding PL peak energies. For all panels the symbols correspond to the experimental data, while the curves show the results of calculations. Only the contribution to the ZPL emission via the admixture of the $\pm 1^L$ bright exciton is taken into account. The populations of the dark exciton states ± 2 are considered to be determined by the relaxation from the $\pm 1^L$ states.

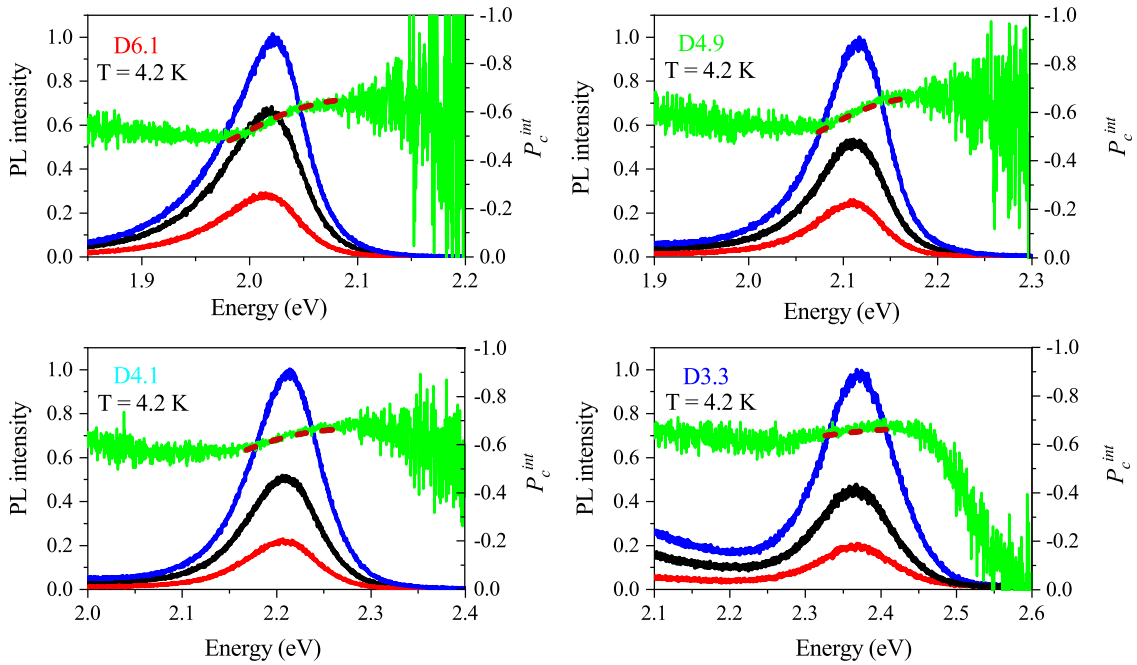


Fig. S22 PL spectra of the σ^+ (red) and σ^- (blue) polarized components at $B = 30$ T and PL spectrum at $B = 0$ T (black). Green line shows the experimental spectral dependence of the circular polarization degree at $B = 30$ T. Red dashed line shows the calculated spectral dependence of the DCP at $B = 30$ T with accounting for the ZPL emission via the admixture of the $\pm 1^L$ bright excitons solely. The populations of the dark exciton states ± 2 are considered to be determined by the relaxation from the $\pm 1^L$ states.

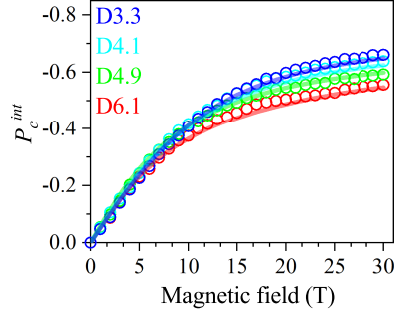


Fig. S23 Magnetic field dependences of the $P_c^{int}(B)$ measured at the PL maximum in all samples. Lines are fits with Eq. 3. The contribution to the ZPL emission via the admixture of the 0^U bright exciton is taken into account. The populations of the dark exciton states ± 2 are considered to be determined by the relaxation from the $\pm 1^L$ states.

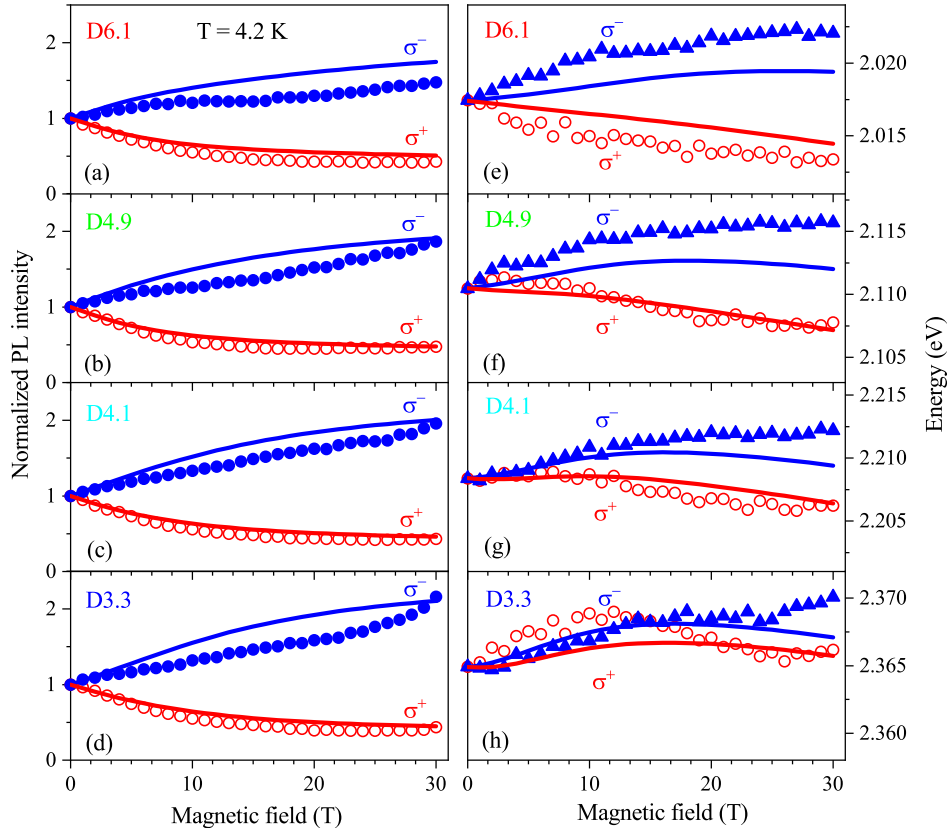


Fig. S24 PL intensity and spectral shifts in magnetic field. (a-d) Time-integrated intensity of the σ^+ (red) and σ^- (blue) polarized PL as function of the magnetic field in CdSe NCs. (e-h) Magnetic field dependences of the corresponding PL peak energies. For all panels the symbols correspond to the experimental data, the curves show the results of calculations. The emission of the dark excitons at the ZPL energy via the admixture of the 0^U bright exciton is included. The populations of the dark exciton states ± 2 are considered to be determined by the relaxation from the $\pm 1^L$ states.

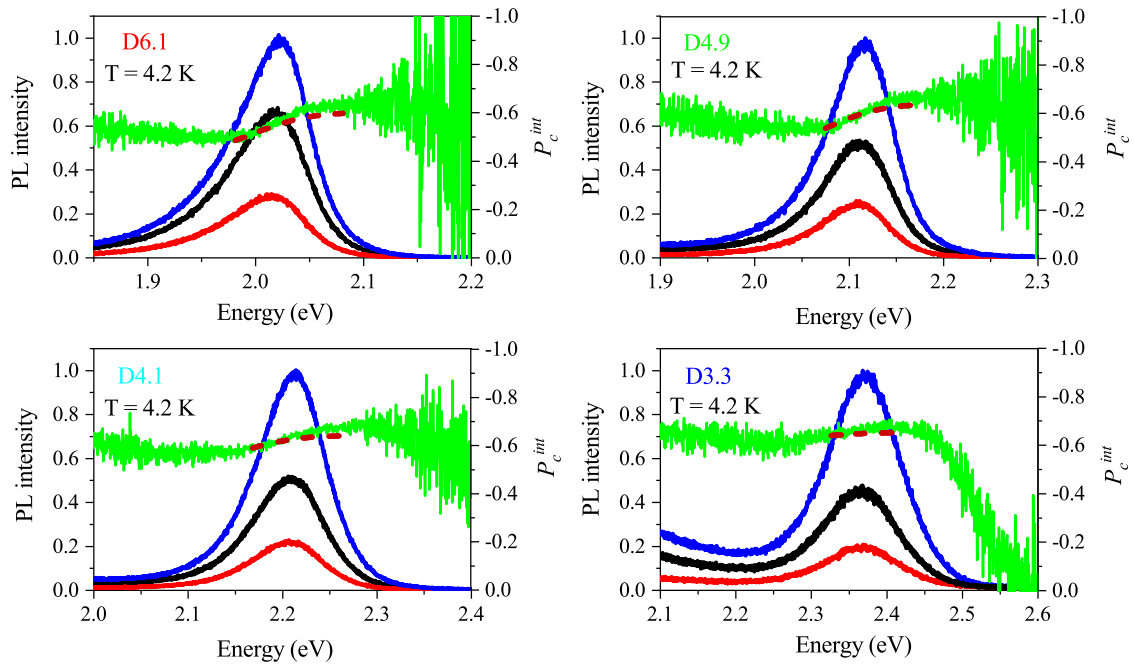


Fig. S25 PL spectra of the σ^+ (red) and σ^- (blue) polarized components at $B = 30$ T and PL spectrum at $B = 0$ T (black). Green line shows the experimental spectral dependence of the circular polarization degree at $B = 30$ T. Red dash line shows the calculated spectral dependence of the DCP at $B = 30$ T. The emission of the dark excitons at the ZPL energy via the admixture of the 0^U bright exciton is included. The populations of the dark exciton states ± 2 are considered to be determined by the relaxation from the $\pm 1^L$ states.

S4.8 Dark exciton and hole g -factors determined from fitting

In Figure S27 we show the dark exciton and hole g -factors determined from fitting of the experimental data. These g -factors are related to each other by the equation $g_h = (g_e - g_F)/3$. Here g_e is electron g -factor. The size dependence of the electron g -factor (see Figure S26) is well studied and can be found in Refs. 18–20. One can see in Figure S27 that the consideration of the linearly polarized ZPL emission and the non-equilibrium population of the dark exciton states significantly modifies the derived dark exciton g -factor (from ≈ 1.6 to ≈ 5) and hole g -factor (from ≈ -0.1 to ≈ -1.4). These results indicate that the value of the hole g -factor determined from the analysis of the polarized PL under nonresonant excitation depends on the number of considered recombination channels of the dark exciton and its spin relaxation.

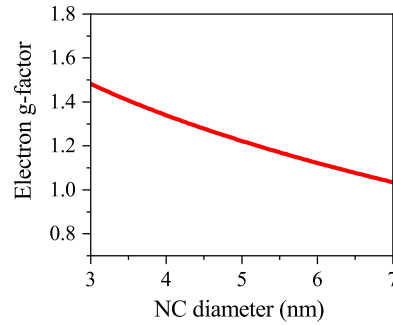


Fig. S26 Size dependence of the electron g -factor in CdSe NCs according to Refs. 18–20.

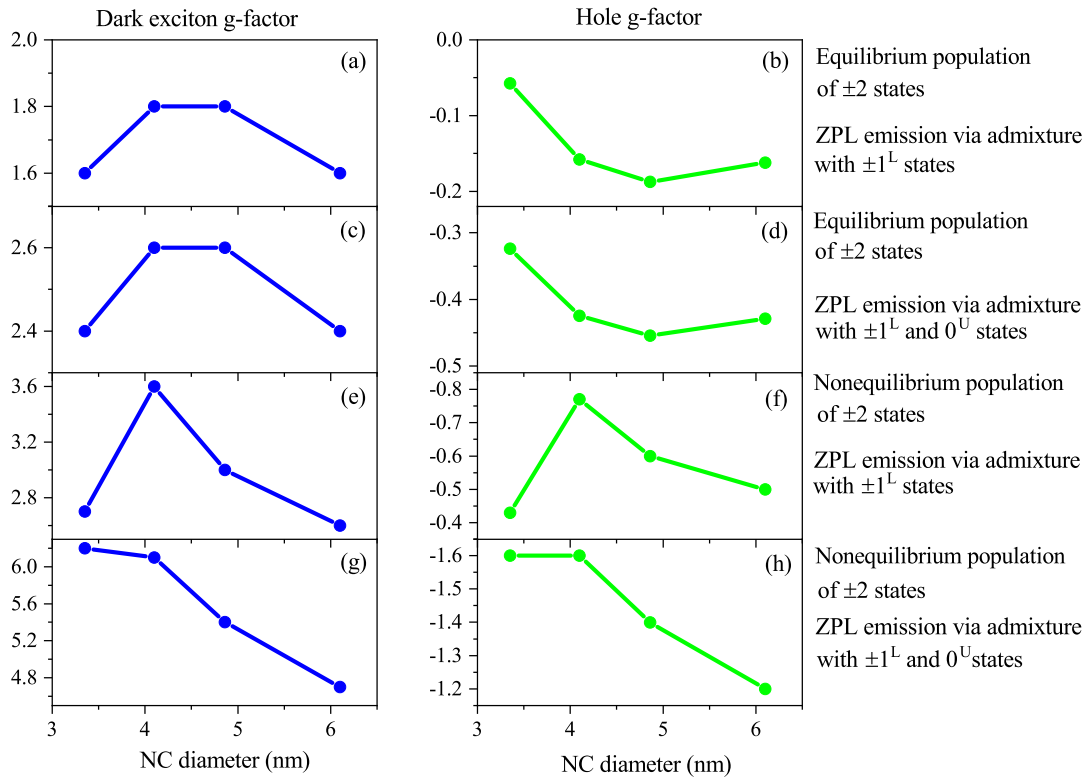


Fig. S27 Size dependence of the dark exciton and hole g -factors determined from fits using the following assumptions: (a,b) Fast spin relaxation between the ± 2 states and ZPL emission via the $\pm 1^L$ admixture; (c,d) Fast spin relaxation between the ± 2 states and ZPL emission via the $\pm 1^L$ and 0^U admixture; (e,f) Slow spin relaxation between the ± 2 states and ZPL emission via the $\pm 1^L$ admixture; (g,h) Slow spin relaxation between the ± 2 states and ZPL emission via the $\pm 1^L$ and 0^U admixture.

References

- 1 Ekimov, A. I.; Hache, F.; Schanne-Klein, M. C.; Ricard, D.; Flytzanis, C.; Kudryavtsev, I. A.; Yazeva, T. V.; Rodina, A. V.; Efros, Al. L. Absorption and intensity-dependent photoluminescence measurements on CdSe quantum dots: assignment of the first electronic transitions, *J. Opt. Soc. Am. B* **1993**, *10*, 100–107.
- 2 Park, Y.-S.; Lim, J.; Klimov, V. I. Asymmetrically strained quantum dots with non-fluctuating single-dot emission spectra and sub-thermal room-temperature linewidths, *Nat. Mater.* **2019**, *18*, 249–255.
- 3 Norris, D. J.; Bawendi, M. G. Measurement and assignment of the size-dependent optical spectrum in CdSe quantum dots, *Phys. Rev. B* **1996**, *53*, 16338–16346.
- 4 Labeau, O.; Tamarat, P.; Lounis, B. Temperature dependence of the luminescence lifetime of single CdSe/ZnS quantum dots, *Phys. Rev. Lett.* **2003**, *90*, 257404.
- 5 Shornikova, E. V.; Golovatenko, A. A.; Yakovlev, D. R.; Rodina, A. V.; Biadala, L.; Qiang, G.; Kuntzmann, A.; Nasilowski, M.; Dubertret, B.; Polovitsyn, A.; Moreels, I.; Bayer, M. Surface spin magnetism controls the polarized exciton emission from CdSe nanoplatelets, *Nat. Nanotechnol.* **2020** *15*, 277–282.
- 6 Efros, Al. L.; Rosen, M.; Kuno, M.; Nirmal, M.; Norris, D. J.; Bawendi, M. Band-edge exciton in quantum dots of semiconductors with a degenerate valence band: Dark and bright exciton states, *Phys. Rev. B* **1996**, *54*, 4843–4856.
- 7 Goupalov, S. V.; Ivchenko, E. L. The fine structure of excitonic levels in CdSe nanocrystals, *Phys. Solid State* **2000**, *42*, 2030–2038.
- 8 Norris, D. J.; Efros, Al. L.; Rosen, M.; Bawendi, M. G. Size dependence of exciton fine structure in CdSe quantum dots, *Phys. Rev. B* **1996**, *53*, 16347–16354.
- 9 Woggon, U.; Gindele, F.; Wind, O.; Klingshirn, C. Exchange interaction and phonon confinement in CdSe quantum dots, *Phys. Rev. B* **1996**, *54*, 1506–1509.
- 10 Chamarro, M.; Gourdon, C.; Lavallard, P.; Lublinskaya, O.; Ekimov, A. I. Enhancement of electron-hole exchange interaction in CdSe nanocrystals: A quantum confinement effect, *Phys. Rev. B* **1996**, *53*, 1336–1342.
- 11 Liu, F.; Rodina, A. V.; Yakovlev, D. R.; Greilich, A.; Golovatenko, A. A.; Susha, A. S.; Rogach, A. L.; Kusrayev, Y. G.; Bayer, M. Exciton spin dynamics of colloidal CdTe nanocrystals in magnetic fields, *Phys. Rev. B* **2014**, *89*, 115306.
- 12 Liu, F.; Biadala, L.; Rodina, A. V.; Yakovlev, D. R.; Dunker, D.; Javaux, C.; Hermier, J.-P.; Efros, Al. L.; Dubertret, B.; Bayer, M. Spin dynamics of negatively charged excitons in CdSe/CdS colloidal nanocrystals, *Phys. Rev. B* **2013**, *88*, 035302.
- 13 Johnston-Halperin, E.; Awschalom, D. D.; Crooker, S. A.; Efros, Al. L.; Rosen, M.; Peng, X.; Alivisatos, A. P. Spin spectroscopy of dark excitons in CdSe quantum dots to 60 T, *Phys. Rev. B* **2001**, *63*, 205309.
- 14 Furis, M.; Hollingsworth, J. A.; Klimov, V. I.; Crooker, S. A. Time- and polarization-resolved optical spectroscopy of colloidal CdSe nanocrystal quantum dots in high magnetic fields, *J. Phys. Chem. B* **2005**, *109*, 15332–15338.
- 15 Wijnen, F. J. P.; Blokland, J. H.; Chin, P. T. K.; Christianen, P. C. M.; Maan, J. C. Competition between zero-phonon and phonon-assisted luminescence in colloidal CdSe quantum dots, *Phys. Rev. B* **2008**, *78*, 235318.
- 16 Del Águila, A. G.; Pettinari, G.; Groeneveld, E.; De Mello Donegá, C.; Vanmaekelbergh, D.; Maan, J. C.; Christianen, P. C. M. Optical spectroscopy of dark and bright excitons in CdSe nanocrystals in high magnetic fields, *J. Phys. Chem. C* **2017**, *121*, 23693–23704.
- 17 Rodina, A. V.; Efros, Al. L. Radiative recombination from dark excitons in nanocrystals: Activation mechanisms and polarization properties, *Phys. Rev. B* **2016**, *93*, 155427.
- 18 Gupta, J. A.; Awschalom, D. D.; Efros, Al. L.; Rodina, A. V. Spin dynamics in semiconductor nanocrystals, *Phys. Rev. B* **2002**, *66*, 125307.
- 19 Hu, R.; Yakovlev, D. R.; Liang, P.; Qiang, G.; Chen, C.; Jia, T.; Sun, Z.; Bayer, M.; Feng, D. Origin of two Larmor frequencies in the coherent spin dynamics of colloidal CdSe quantum dots revealed by controlled charging, *J. Phys. Chem. Lett.* **2019**, *10*, 3681–3687.
- 20 Tadjine, A.; Niquet, Y.-M.; Delerue, C. Universal behavior of electron g-factors in semiconductor nanostructures, *Phys. Rev. B* **2017**, *95*, 235437.
- 21 Biadala, L.; Louyer, Y.; Tamarat, P.; Lounis, B. Band-edge exciton fine structure of single CdSe/ZnS nanocrystals in external magnetic fields, *Phys. Rev. Lett.* **2010**, *105*, 157402.
- 22 Efros, Al. L. Chapter 3 on Fine structure and polarization properties of band-edge excitons in semiconductor nanocrystals, in *Semiconductor and Metal Nanocrystals: Synthesis and Electronic and Optical Properties*, Edited by Klimov, V. I. (Marcel Dekker, New York, 2003) pp. 97–132.